STScI | SPACE TELESCOPE SCIENCE INSTITUTE

Instrument Science Report WFC3 2023-03

WFC3/UVIS: 2021 and 2022 Superbias Reference File Procedural Updates

I. Rivera, B. Kuhn
May 31, 2023

ABSTRACT

In this report we discuss the modified procedure for generating a superbias reference file for the Wide Field Camera 3 (WFC3) UVIS detector. Changes to the procedure include processing bias files individually, flagging cosmic rays, and replacing undefined (NaN) values. We compare the 2020 superbias currently in the Calibration Reference File System (CRDS) to a 2020 superbias created using the new procedure. We find a negligible increase of $0.02 \pm 0.10\ e^-$ *in the average 2020 superbias level compared to the original procedure and thus will not deliver a new version of the 2020 reference file to CRDS. The 2021 and 2022 superbiases were generated using the updated procedure and we compare the 2022 superbias to the 2020 CRDS superbias in this report. The 2022 average superbias value is* $0.34 \pm 0.07\ e^-$ *for UVIS 1 and* $0.39 \pm 0.07\ e^-$ *for UVIS 2. We analyzed the superbias level from 2009 to 2022 per readout amplifier, finding a gradual increase due to dark current accumulated during readout and charge transfer efficiency losses in the detector. The current rate of increase per chip is* $0.016 \pm 0.001\ e^-/year$ *and* $0.033 \pm 0.002\ e^-/year$ *for UVIS 1 and 2 respectively. The 2021 and 2022 superbias reference files have been delivered to CRDS and are in use in the calibration pipeline. Observers can request updated products through the Mikulski Archive for Space Telescopes (MAST).*

1. Introduction

The Wide Field Camera 3 (WFC3) UVIS detector is comprised of two charge-coupled devices (CCDs) UVIS 1 and UVIS 2. Positioned at the outer corners of each CCD, or chip, are two readout amplifiers: A and B for UVIS 1, and C and D for UVIS 2. The default readout mode commands each amplifier to read out signal from a corresponding quadrant of the detector, simultaneously (Figure 1). During readout, the charge packet in each pixel is transferred row-by-row down the detector, in parallel to the serial register, which is located along the side of the chip with the amplifiers. Each amplifier is commanded with a bias offset to help avoid negative pixel values during readout, and is denoted in the `BIASLEVA-D` primary header keywords. Bias frames

are 0-second exposures with the shutter closed, and are taken throughout the year to monitor the initial pixel values and read noise in the detector. At the end of the year, these exposures are combined to create a final superbias image, which is used to subtract the residual bias from all WFC3 UVIS images taken in that period.

All calibrated WFC3 data in MAST are processed through the calibration pipeline called `calwf3`. `calwf3` performs the UVIS bias correction in two steps, the overscan correction and superbias correction, which are invoked by the keywords `BLEVCORR` and `BIASCORR` respectively. During the `BLEVCORR` step, the bias level is measured in the overscan regions of the raw image and subtracted from the CCD image area (see Figure 1). The overscan regions are areas of the detector where the pixels are unexposed to light, so they provide a measure of the bias level during an exposure. The majority of the bias signal is removed from the image after the overscan correction, and the overscan regions are trimmed in the calibrated FLT image. What is left behind is a two-dimensional residual bias structure that is subtracted from the image using the superbias reference file during the `BIASCORR` step. Currently, a superbias file is created for each year by combining approximately 50 bias frames taken throughout the corresponding year. For more information concerning `calwf3` processing, see Sahu et al. (2021).

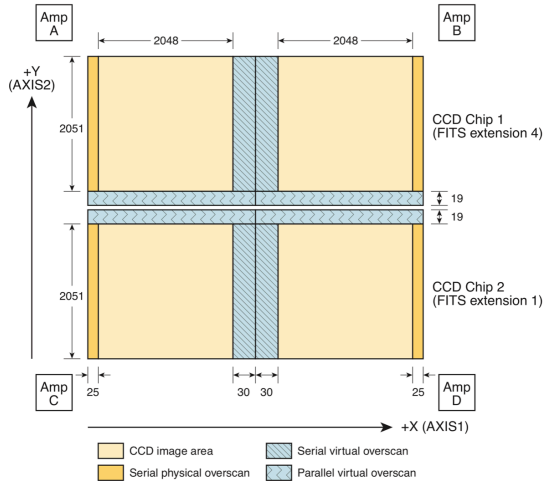

Figure 1. Schematic of a raw, full-frame WFC3 UVIS image. Each detector quadrant is read by the associated amplifier located in each corner. There are 19 rows of parallel virtual overscan by the chip gap and 30 columns of virtual overscan at the inside y-edge. There are also 25 columns of serial physical overscan on the outside y-edges of each quadrant. For every UVIS image, the bias level is computed in these regions and subtracted from the CCD image area. The calibrated FLT or FLC images have the overscan regions removed. (Sahu et al., 2021)

In this work, we generate the 2021 and 2022 superbias reference files using an updated version of the procedure discussed in Instrument Science Report (ISR) WFC3 2019-11 (Kuhn and Khandrika, 2019), where the authors created the 2018 superbias reference file (the 2019 and 2020 superbiases were generated with this procedure as well). In Section 2, we describe how we obtained and prepared the data. In Section 3, we discuss the modified procedure for processing and combining bias files to generate the superbias. Section 4 provides an analysis of the modified and former procedure with the last delivered superbias before this work, the 2020 superbias.

Section 5 compares the 2020 superbias in CRDS with the 2022 superbias created with the updated procedure. In Section 7 we analyze the bias level of all 15 superbiases from 2009-2022. Section 8 discusses how we validated the 2021 and 2022 superbiases, and how to access the modified code. Finally, Section 9 summarizes the results.

2. Data

We retrieved all the raw bias files taken throughout the year (January 1 – December 31). There are approximately 4 bias exposures taken per month, two before and after each anneal. The 2021 WFC3 UVIS superbias files were generated using bias exposures from the HST Cycle 28 and 29 monitoring programs 16414 and 16564. The 2022 WFC3 UVIS superbias files were generated using bias exposures from the HST Cycle 29 and 30 monitoring programs 16564 and 16967. All our bias files are 0-second, full-frame, unbinned exposures with no post-flash or charge injection. We ran the CRDS tool, `bestref`, to update the file headers with the latest reference files and tables. All the bias files used to create each superbias are listed in the HISTORY section of the superbias primary header. Table 1 provides the Program IDs and Cycle numbers for the bias data we retrieved in 2021 and 2022.

Superbias Year	Proposal ID	Cycle
2021	16414	28
	16564	29
2022	16564	29
	16967	30

Table 1. The Proposal IDs and HST Cycle numbers of the bias data used to generate the 2021 and 2022 superbias reference files.

3. Modified Procedure for Creating a Superbias Reference File

The 2021 and 2022 superbiases were created using a similar procedure as Kuhn and Khandrika (2019): we retrieved all raw full-frame biases taken in the given year, processed them through the `calwf3` pipeline to perform overscan subtraction, flagged cosmic rays (CRs) in the FLT Data Quality (DQ) arrays, used the DQ arrays to mask the science and error arrays, and finally average combined the science arrays and propagated the error arrays. We modified the existing superbias scripts to adjust the methods for three of these steps, as detailed below (and quantified in Section 4).

The previous method provided `calwf3` with an association (ASN) table listing the rootnames of all the raw bias files, which enables them to be processed together. Providing an asn table also initializes the `CRCORR` step, which prompts the subroutine `wf3rej` to perform CR rejection. When bias files are constructed in an asn table they are assigned as member type `CR-SPLIT`. `calwf3` processes `CR-SPLIT` exposures by retrieving the calibration switch and reference file keyword settings from the first image listed, and applying them to the rest of the set (Sahu et al., 2021). However, bias files can be assigned different reference files (e.g. bad

pixel tables) depending on when they were taken throughout the year, thus the asn process (where the reference files from the first image listed are applied to all images in the association) is not ideal. The updated procedure calls `calwf3` on the raw files individually to ensure each file's assigned reference files are applied, and the `wf3rej` subroutine is not invoked. We processed the bias files individually for the 2021 and 2022 superbiases, and the bias files used to generate the 2009-2020 superbias were processed in an association.

The second change from the previous procedure is the method for CR flagging and removing extreme outliers. The previous method called `calwf3`'s `wf3rej` subroutine to identify and flag CRs in the FLT DQ arrays. In addition, the previous superbias code dilated the CR pixels by a 5-pixel radius to mask charge transfer efficiency (CTE) trails, and extreme outliers were removed by performing three iterations of 3σ-clipping on the average pixel value across each chip in the dataset. If there was an outlier, then the entire image was clipped from the set. The updated procedure now runs a custom CR-flagging script that compiles all calibrated FLT science arrays into a single data cube for both UVIS 1 and UVIS 2, and performs three iterations of 3σ-clipping on a pixel-by-pixel basis through the z-axis. To mitigate the CTE trails from the CRs, an extra 10 pixels are flagged in the anti-readout direction. Since the new algorithm performs sigma-clipping on a pixel-by-pixel basis we can efficiently mask extreme-outlier pixels instead of clipping out an entire image. This allows us to use all the available bias images from a given year to generate the superbias.

The final procedural adjustment we made is the method for setting the values of the bad pixels and columns in the superbias. The DQ arrays mask bad pixels in the science and error arrays of the FLT files by setting any pixel that has a nonzero value in the DQ array to NaN for the corresponding science array pixel. These pixels are ignored when the science arrays are average-combined. In the prior method, the NaN pixels in the combined image were converted to zero. Now we replace them with the mean of the surrounding pixels contained within a 31x31 stamp centered on the NaN pixel. Table 2 summarizes the three revised methods described in this section.

Method Changed	**Superbiases 2009 - 2020 (Previous procedure)**	**Superbiases 2021 - present (New procedure)**	**Benefit**
Processing RAW Bias Files	Processed by `calwf3` in an association table. Reference files from first exposure applied to all images.	Processed by `calwf3` individually. Each image has their specific reference files applied.	Bias files will have their own unique reference files and tables (e.g. bad pixel tables) applied during `calwf3` processing.
Flagging Cosmic Rays and Removing Extreme Outliers	1. Flagged by `wf3rej` subroutine during `calwf3`'s `CRCORR` step. 2. 5-pixel radius dilation. 3. 3σ-clipping on average chip value.	1. Flagged by per-pixel sigma clipping with thresholding. 2. 10-pixels flagged in anti-readout direction.	Entire file set is always used to create the superbias. Less over-flagging of pixels surrounding CRs.
Replacing Undefined NaN Pixels	All NaN pixels replaced with zero.	Each NaN pixel replaced with mean of a stamp centered at the pixel.	Better approximation of bad pixel values.

Table 2. Modified methods in the procedure for processing bias files to generate the superbias.

4. 2020 Superbias Comparison: New vs Old Procedure

We recreated the 2020 superbias with the new methods outlined in Table 2. The top row in Figure 2 displays histograms of the UVIS 1 (left) and UVIS 2 (right) pixel values for both the original 2020 superbias in CRDS (labeled *CRDS* in Figure 2) and the 2020 superbias created with the revised procedure (labeled *New* in Figure 2). The bottom row of plots in Figure 2 shows pixel values for the difference image of the original superbias subtracted from the newly created superbias. The average pixel difference is $0.01 \pm 0.09\ e^-$ and $0.02 \pm 0.10\ e^-$ for UVIS 1 and 2 respectively.

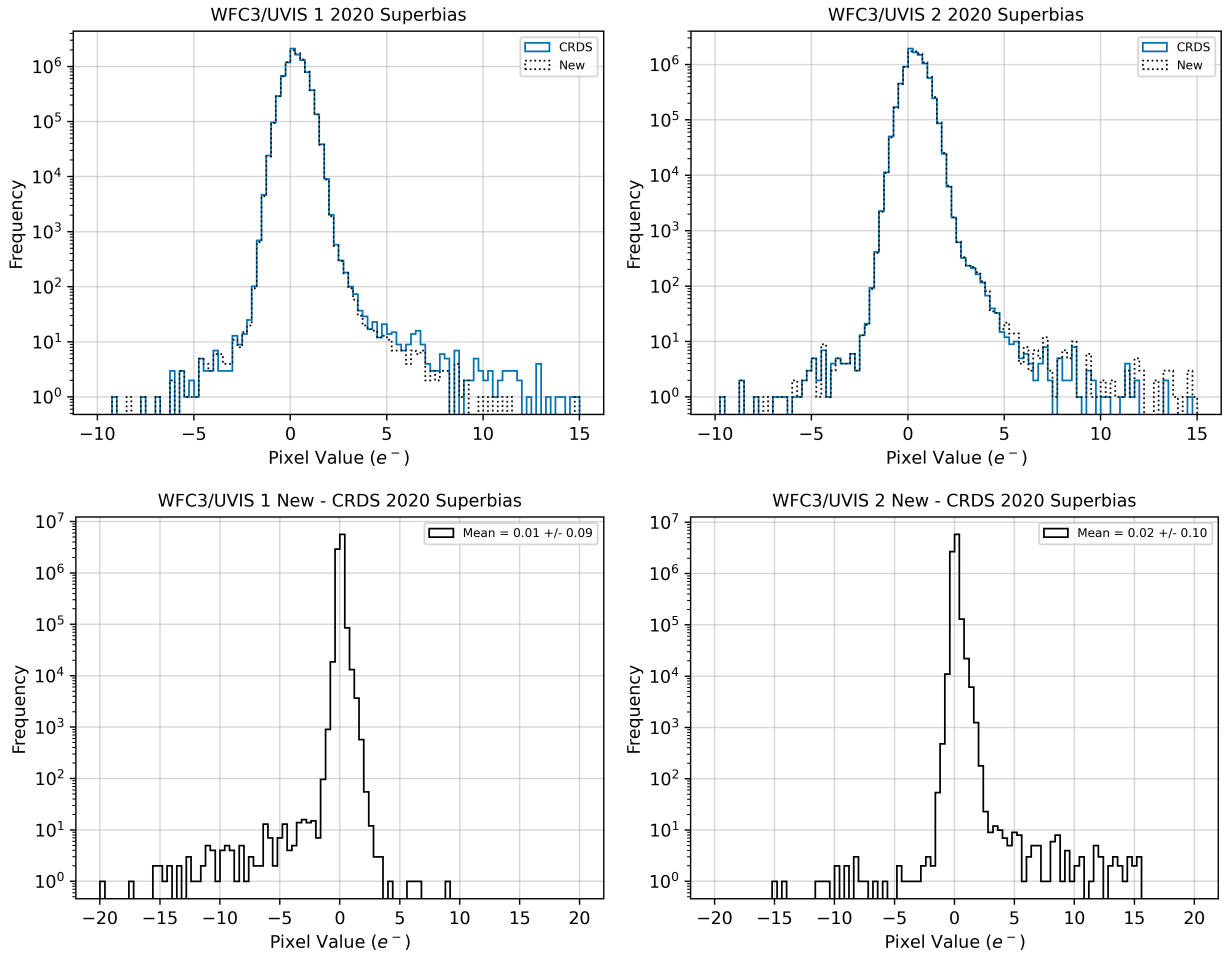

Figure 2. Top row: A histogram of the 2020 superbias currently in CRDS (*CRDS*) and the 2020 superbias created using the new procedure (*New*) for UVIS 1 and 2. Bottom row: The residual histogram of the new 2020 superbias minus the 2020 CRDS superbias. The mean difference is $0.01 \pm 0.09\ e^-$ for UVIS 1 and $0.02 \pm 0.10\ e^-$ for UVIS 2. This corresponds to a ~4% increase in the average bias for UVIS 1 and a ~5% increase for UVIS 2.

To determine the impact of all three revisions to the superbias creation procedure, we created three versions of the 2020 superbias to track each stage of implemented changes:

processing the bias files separately, CR-flagging using our custom method, and interpolating NaN pixels instead of setting them to zero. We created a version of the superbias using the old procedure, but with the bias files processed separately (labeled *sep files* in Figure 3). We also created a version with this correction and the new CR flagging method, but set the NaN pixels in the average combined file to zero (labeled *sep&CR* in Figure 3), as was originally done in Kuhn and Khandrika (2019). Finally, we created a superbias applying all three updated methods – bias files processed separately, new CR flagging method, and interpolated NaN pixels (labeled *New* in Figure 3). Figure 3 shows the 2020 superbias histogram after each stage, with the bottom row of plots showing the histograms of the superbias difference images after each revision is subtracted by the one prior.

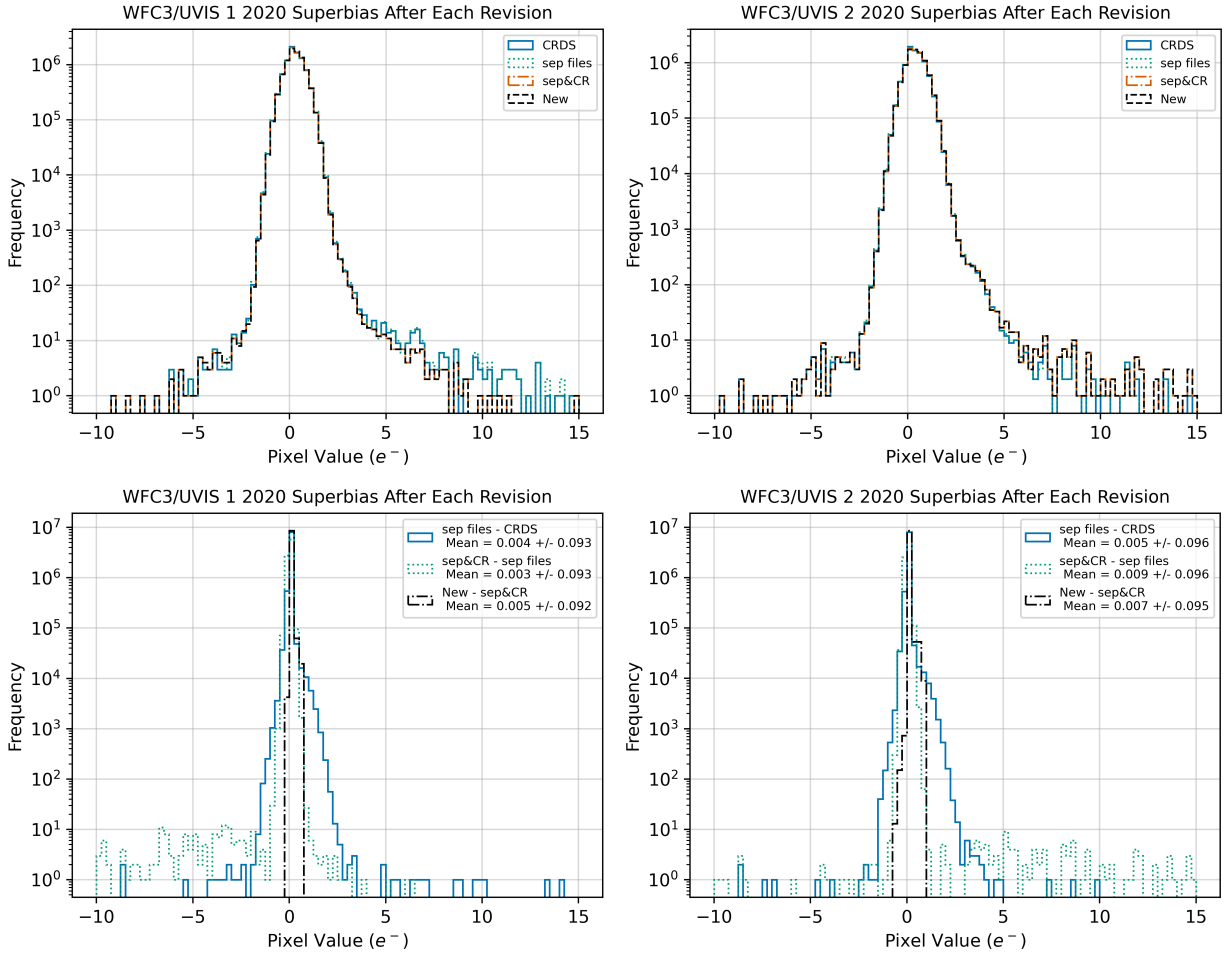

Figure 3. Top row: A histogram of the 2020 superbias before and after each new revision: the superbias currently in CRDS (*CRDS*), with the bias files processed separately (*sep files*), with the new CR flagging method (*sep&CR*) and the final new superbias with all previous revisions plus mean interpolation of the NaNs pixels (*New*). Bottom row: The difference histograms after each new revision. **Note:** The sum of the differences in the average mean is ~0.01 e^- for UVIS 1 and ~0.02 e^- for UVIS 2, which is approximately equal to the total average increase of the superbias before and after implementing the new procedure for each chip (see plots in bottom row of Figure 1).

Figure 4 shows the percent contribution of each revised method on the total increase of the 2020 superbias average value from the old to updated procedure. Separately processing the bias files contributed to ~33% of the total increase of the average pixel value for UVIS 1 and ~24% of the total increase for UVIS 2. The new CR flagging method accounts for ~25% and ~43% of the total increase for UVIS 1 and 2 respectively. The NaN interpolation contributes to 42% of the total increase in UVIS 1 and 33% of the total increase for UVIS 2. For UVIS 1, the mean NaN interpolation contributed to the largest average increase in the superbias while the new CR flagging method added the largest average increase for UVIS 2. Since these changes have a minor impact on the 2020 superbias (overall < 5% increase) there is no plan to regenerate and redeliver the 2009-2020 superbiases to CRDS. These procedural changes have been adopted as the new standard and will be used to generate all superbiases from 2021 onward.

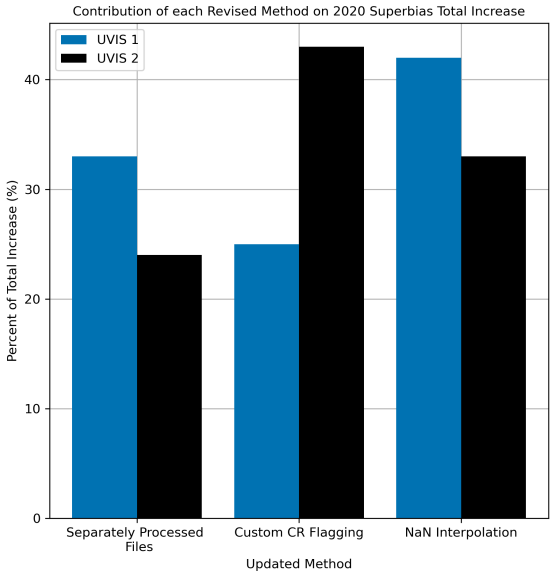

Figure 4. The percent contribution of each revision of the superbias creation procedure on the total increase of the 2020 superbias average value.

3.1 2020 Superbias Comparison: New vs Old CR Flagging

The previous method for CR flagging utilized the `wf3rej` subtask called by `calwf3` when the `CRCORR` switch is set to PERFORM in the primary header of a RAW UVIS file. `wf3rej` is a robust procedure that utilizes a statistical detection algorithm to determine the deviation of each pixel within an input image (Sahu et al., 2021). Pixels within a 2.1 radius of a CR are also flagged with the 8192 value in the FLT DQ array. The previous bias scripts further dilated these pixels by a 5-pixel radius to mitigate the effects of CTE trails. The updated routine for CR flagging uses an iterative sigma-clipping computation (described in Section 3), and only flags pixels that are above a certain user defined threshold, which for the 2021 and 2022 superbiases was 10 DN. Instead of dilating the pixels where CRs are found, we mitigate CTE trails by flagging an additional 10 pixels in the anti-readout direction. We find that this approach flags fewer surrounding pixels as CRs and therefore conserves more data in the average combined superbias. Previously (2009 - 2013), hundreds of biases per year were taken to closely monitor

the instrument's on-orbit behavior. Since 2014, the number of bias observations taken has decreased to approximately 50 exposures per year, so each rejected pixel represents a greater loss to the superbias sample. Figure 5 shows an example comparison between the old and new CR flagging on a CR pixel in a small (30x32) region of UVIS 1.

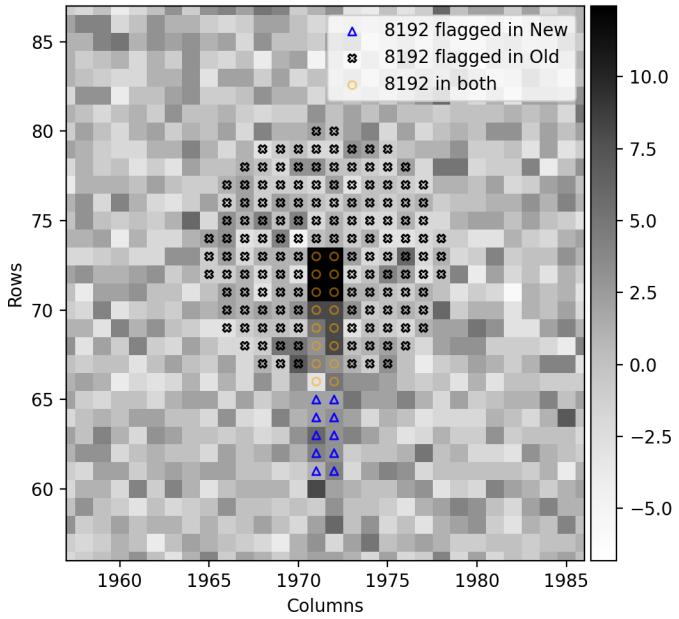

Figure 5. Example of CR flagging using the old (`wf3rej` and radial dilation) and new (pixel-by-pixel sigma-clipping and CTE trail flagging) methods. This image is showing the location of a CR in UVIS 1 of bias image "ie1h21czq". The black "×" markers show all the pixels flagged by the old method. The blue triangle markers show where pixels are flagged by the new method. The orange circle markers show where pixels are flagged by both methods. The old method flags approximately 6 times more pixels than the new CR flagging method for this example.

The new CR flagging method contributes to an extremely small increase in the average superbias level ($0.003 \pm 0.093\ e^-$ and $0.007 \pm 0.096\ e^-$ for UVIS 1 and 2, respectively). To further explore the differences in CR flagging by the new and old method, we performed a similar analysis as Kuhn and Khandrika (2019) by plotting the percentage of the pixels in each chip flagged with CRs in the FLT DQ arrays using each method (Figure 6).

Using the new method, an average of ~230k and ~224k fewer pixels were flagged in the FLT DQ arrays for UVIS 1 and 2, respectively (~2.7% of each chip, see bottom row of Figure 6). The new code takes a more targeted approach to flagging CRs and their CTE trails than the old code did in order to preserve as many good pixels as possible. As a consequence, the superbias level is slightly higher in the new method than the old, but only by a very small amount, consistent with results from Kuhn and Khandrika (2019).

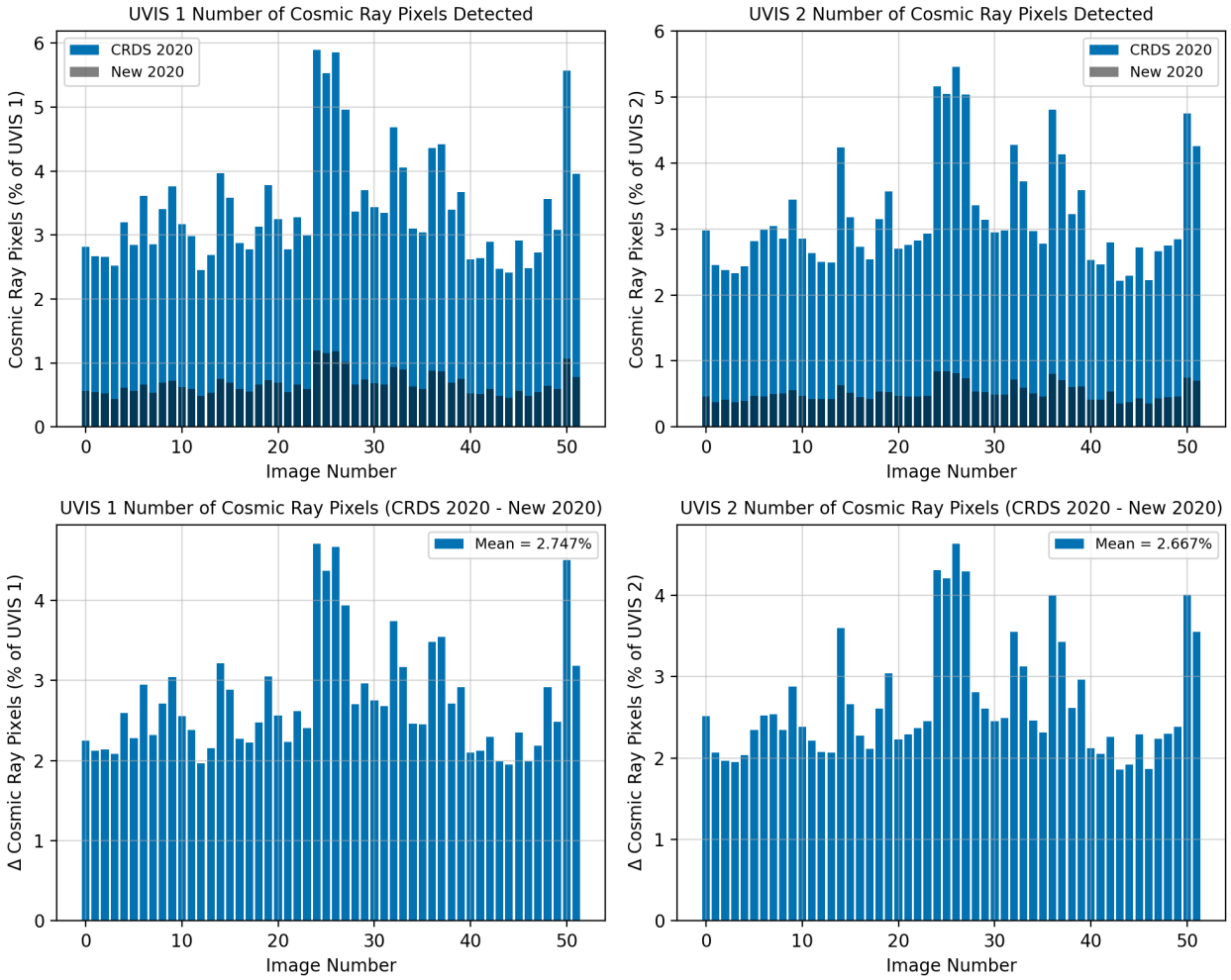

Figure 6. Top row: The number of cosmic ray pixels (and CTE trails) flagged in the FLT DQ arrays of all the 2020 bias files using the old CR flagging procedure (CRDS) and new procedure (New) as a percentage of the total number of pixels in each chip. Bottom row: The percent difference between the number of pixels flagged using the old and new procedure. The new procedure flags about 2.7% fewer pixels in UVIS 1 and 2.

5. 2022 Superbias Analysis

The 2021 and 2022 superbiases were delivered into CRDS for use in the MAST calibration pipeline in April 2023. In this section, we compare the 2022 superbias (generated with the new procedure) to the 2020 CRDS superbias; Figure 7 shows their histograms. The 2022 average pixel value is $0.34 \pm 0.07\ e^-$ and $0.40 \pm 0.07\ e^-$ for UVIS 1 and 2 respectively. The average superbias level from 2020 to 2022 increased in UVIS 1 (by ~23%, $0.06 \pm 0.10\ e^-$) and decreased in UVIS 2 (by ~32%, $0.01 \pm 0.10\ e^-$). To confirm that the drop in the UVIS 2 average superbias pixel value was not solely due to the new procedure, we created the 2022 superbias using the previous procedure and still found a decrease in the UVIS 2 average.

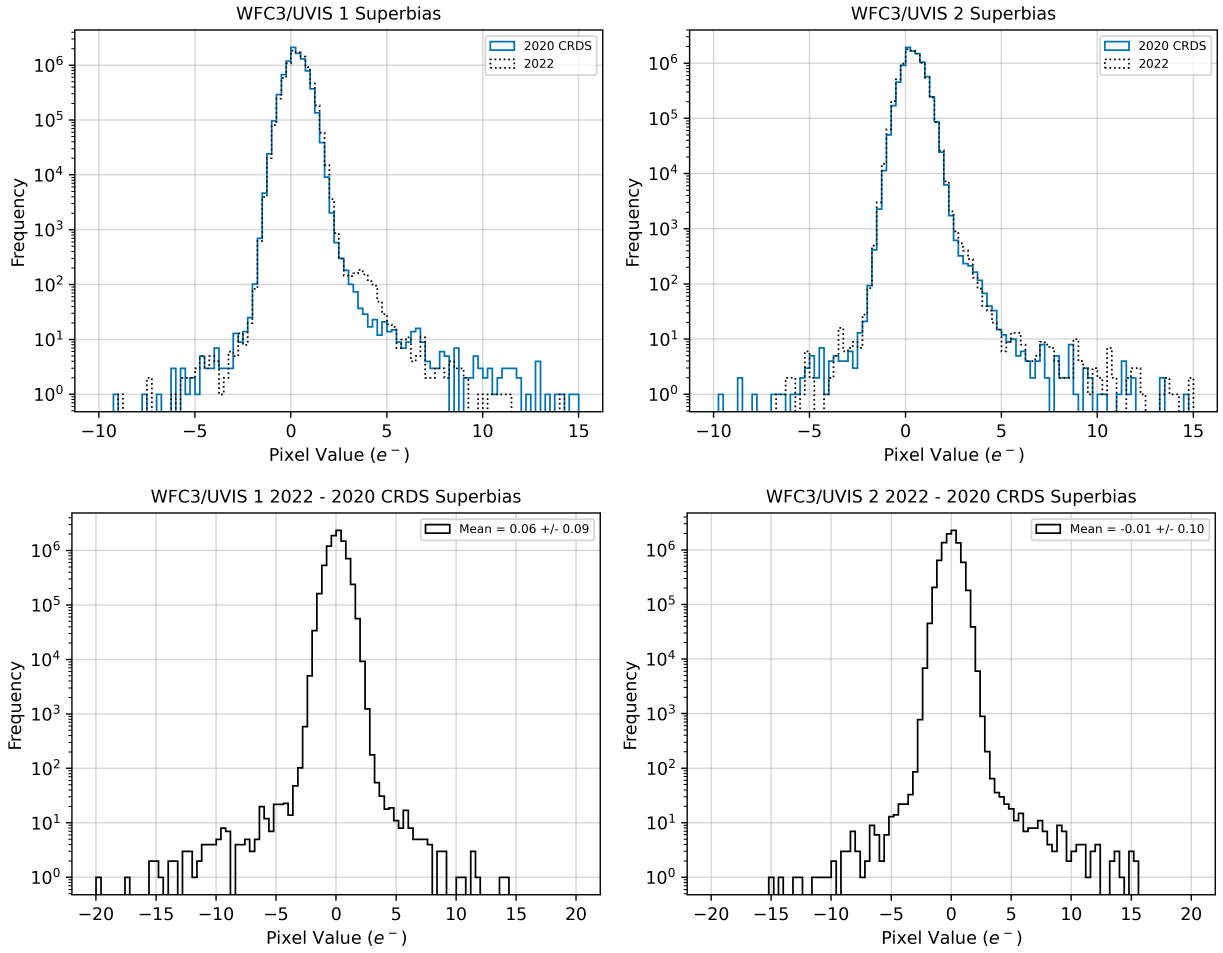

Figure 7. Top row: A histogram of the 2022 superbias and the 2020 superbias in CRDS for UVIS 1 and 2. Bottom row: A histogram of the 2020 CRDS superbias subtracted from the 2022 superbias. The 2022 superbias increased by an average of $0.062 \pm 0.094\ e^-$ for UVIS 1 and decreased by an average of $-0.012 \pm 0.096\ e^-$ for UVIS 2. **Note:** The 2022 superbias was created using the new procedure whereas the 2020 CRDS superbias was created by the old methods for processing the bias files, CR flagging, and replacing the NaN pixels. However, a 2022 superbias generated using the old procedure compared to the CRDS 2020 superbias confirmed the slight decrease in the UVIS 2 superbias level.

To explore how the two-dimensional bias structure is changing, we created cross-section plots by taking the median of each column in UVIS 1 and 2 for the 2020 (CRDS) and 2022 superbias (using the new procedure) (Figure 8). From 2020 to 2022, we see a uniform increase across the chip for UVIS 1 and across the right half of UVIS 2 (amp D). There is a uniform decrease in the column median across the left half of UVIS 2 (amp C). This is an indicator that the average decrease in UVIS 2 is due to lower pixel values in amp C. The overall superbias structure in UVIS 2 for 2020 and 2022 is nominal and although there is a decrease across amp C the average column median has only marginally decreased. We further compared the ratio and difference images which also did not reveal abnormalities.

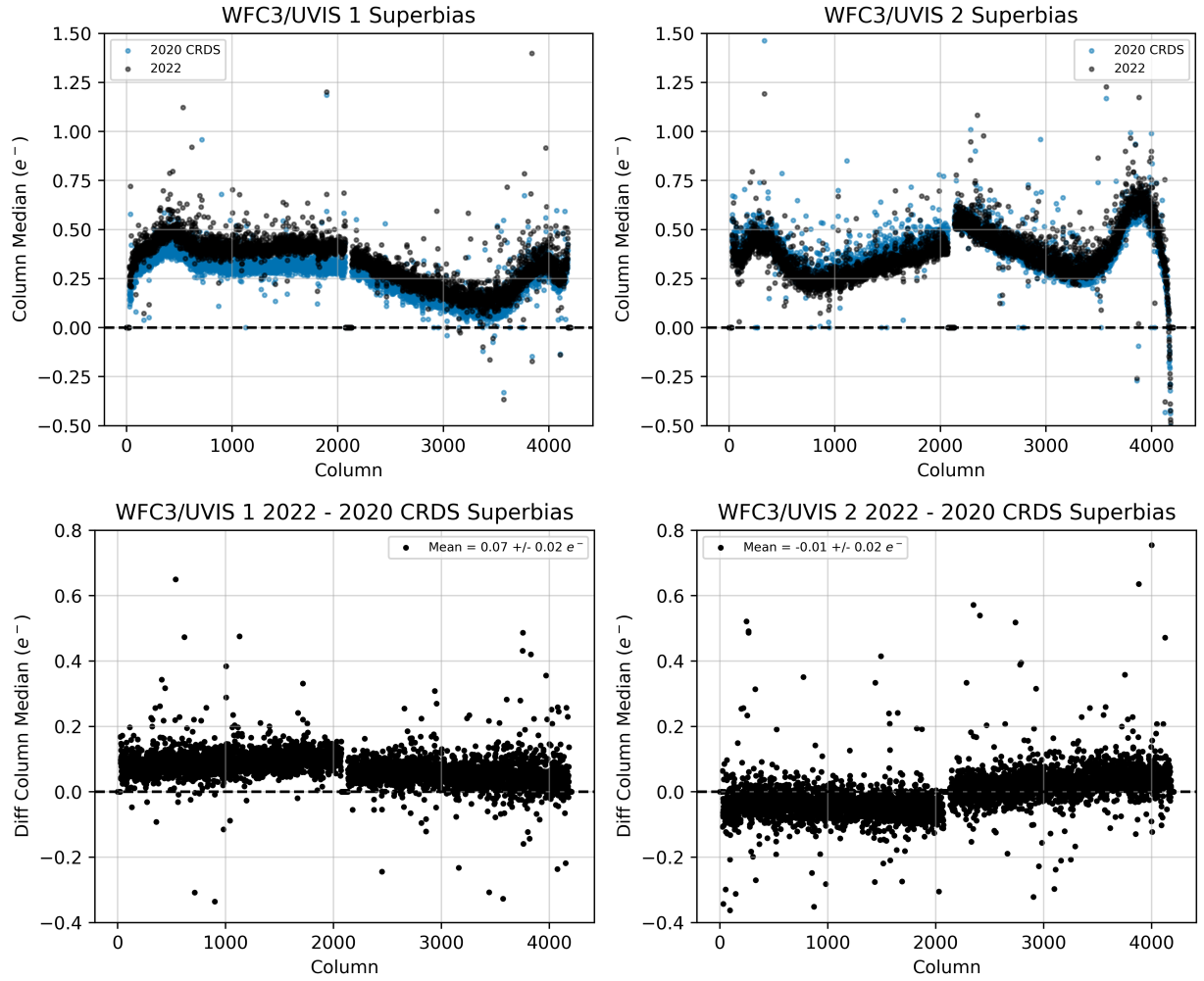

Figure 8. Top row: The 2022 and 2020 CRDS column median plots for UVIS 1 and 2. Bottom row: The difference column median plot of the 2022 and 2020 superbias for UVIS 1 and 2. The black dashed line represents $y = 0$. There is a positive increase in the average column median across UVIS 1 of $0.07 \pm 0.02\ e^-$ and a slight decrease of $-0.01 \pm 0.02\ e^-$ across UVIS 2.

6. Temporal Variations in the 2009-2022 Superbiases

Figure 9 presents the histograms of all 15 superbiases created from 2009-2022, which show the gradual increase in the superbias level over time in both chips. The 2021 and 2022 superbias files were created using the modified procedure discussed in Section 3. The UVIS 2 histogram distribution for the 2015-2018 superbias have a noticable secondary peak of pixels with values between 2.5-5 e^-. In the 2019 and 2020 superbias, the number of these pixel values decreases. A similar secondary peak emerges in UVIS 1 for the 2021 and 2022 superbiases. As previously found by Kuhn and Khandrika (2019) the secondary peaks are mostly due to intermittent bad partial columns. Figure 10 highlights these high value pixels ($\geq 2.5e^-$) revealing the locations of these bad partial columns in UVIS 1 for the 2022 superbias. The appendix also shows where these pixels are in the 2019-2022 superbias, which illustrates the increasing number of bad columns that appear with each superbias.

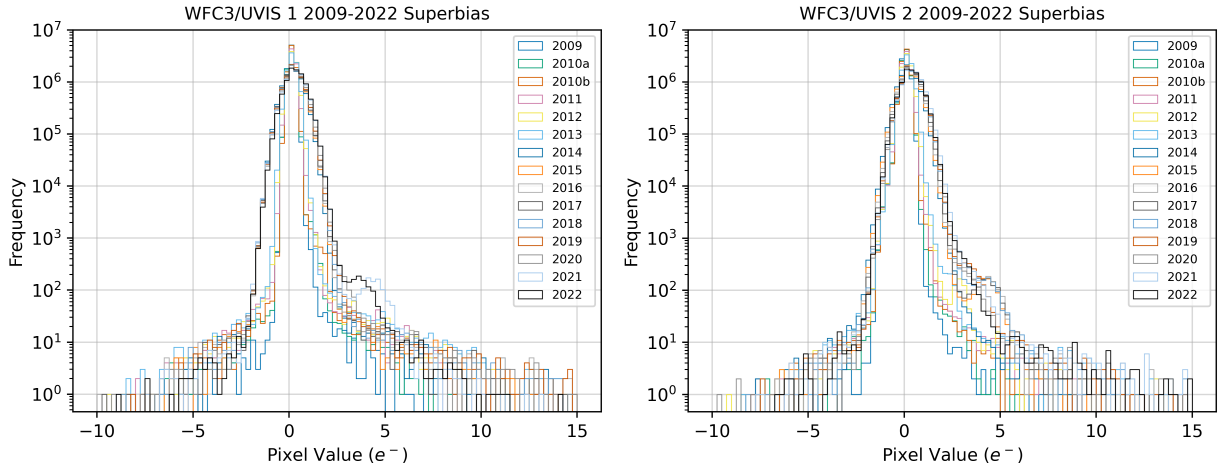

Figure 9. A histogram of superbias pixel values from 2009-2022 for UVIS 1 (left) and 2 (right). The slow increase in the superbias level over time is characterized by the broadening of the pixel distribution. A secondary peak can be seen in the UVIS 1 superbias for years 2021 and 2022, and the UVIS 2 superbias from 2015-2022. The secondary peak in both chips is mostly due to bad partial columns (see Figure 10 and appendix).

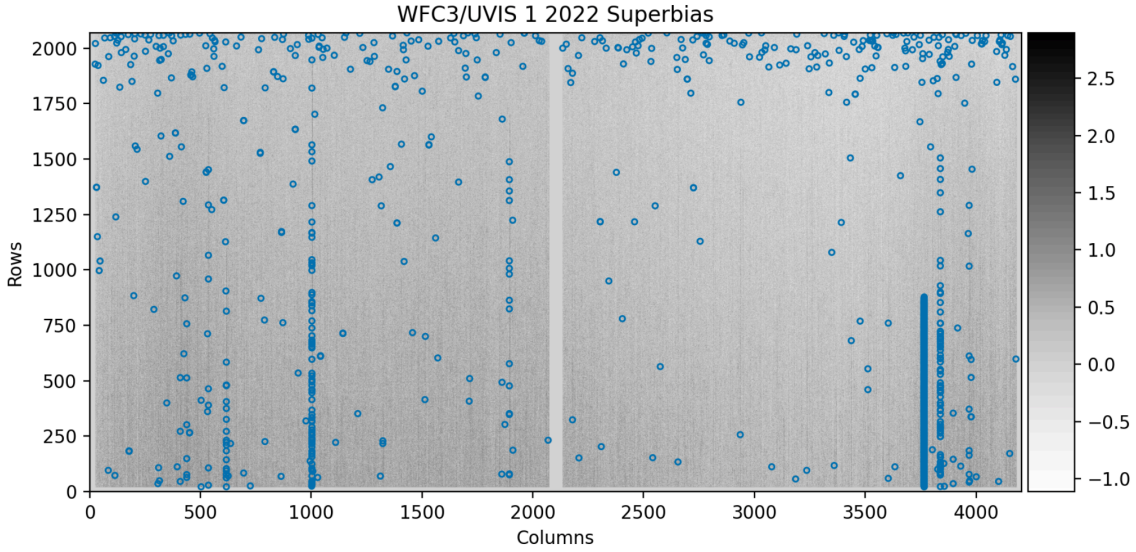

Figure 10. The 2022 superbias for UVIS 1. The locations of pixels with a value >= 2.5 e- are shown with blue apertures. There are 1,403 high value pixels (0.016% of chip) in the 2021 UVIS 1 superbias and 1,496 high value pixels (0.017% of chip) in the 2022 UVIS 1 superbias. The majority of these pixels are located in bad partial columns that come and go intermittently. See the Appendix for full-frame images of the 2019-2022 superbiases marked with the locations of pixels with values $\geq 2.5\ e^-$.

These bad or "hot" partial columns can occur when charge from damaged, hot pixels leak along the columns of the image data during readout. Hot pixels accumulate significantly more dark current than other pixels. As high energy radiation continues to damage the detector, the number

of hot pixels will increase and form more hot columns. Since the number of pixels with a value $\geq 2.5e^-$ only make up 0.016% of the chip, the impact of them on the average superbias value is so far negligible, but will continue to be monitored. If necessary, these intermittent bad columns will be added to the bad pixel table. Meanwhile, dithering science exposures, which the vast majority of observers do, will help mitigate their impact.

We calculated the mean pixel value per amplifier of every superbias since 2009 and plotted it as a function of year in Figure 11. This plot demonstrates the rate of increase in the mean superbias level over time with error bars representing the standard error of the mean. We performed a linear fit to the data and calculated a slope of $0.022 \pm 0.001\ e^-/yr$, $0.009 \pm 0.001\ e^-/yr$, $0.025 \pm 0.002\ e^-/yr$, and $0.041 \pm 0.002\ e^-/yr$ for amp A, B, C, and D respectively. For UVIS 1, amp A is increasing at a $0.013 \pm 0.001\ e^-/yr$ higher rate than amp B, and for UVIS 2, amp D is increasing at a $0.016 \pm 0.003\ e^-/yr$ higher rate than amp C. There is a drop in the average value of the 2022 superbias in UVIS 2 for both amps with a slightly greater drop in amp C. The average rate of increase in the superbias level per chip is $0.016 \pm 0.001\ e^-/yr$ for UVIS 1 and $0.033 \pm 0.002\ e^-/yr$ for UVIS 2.

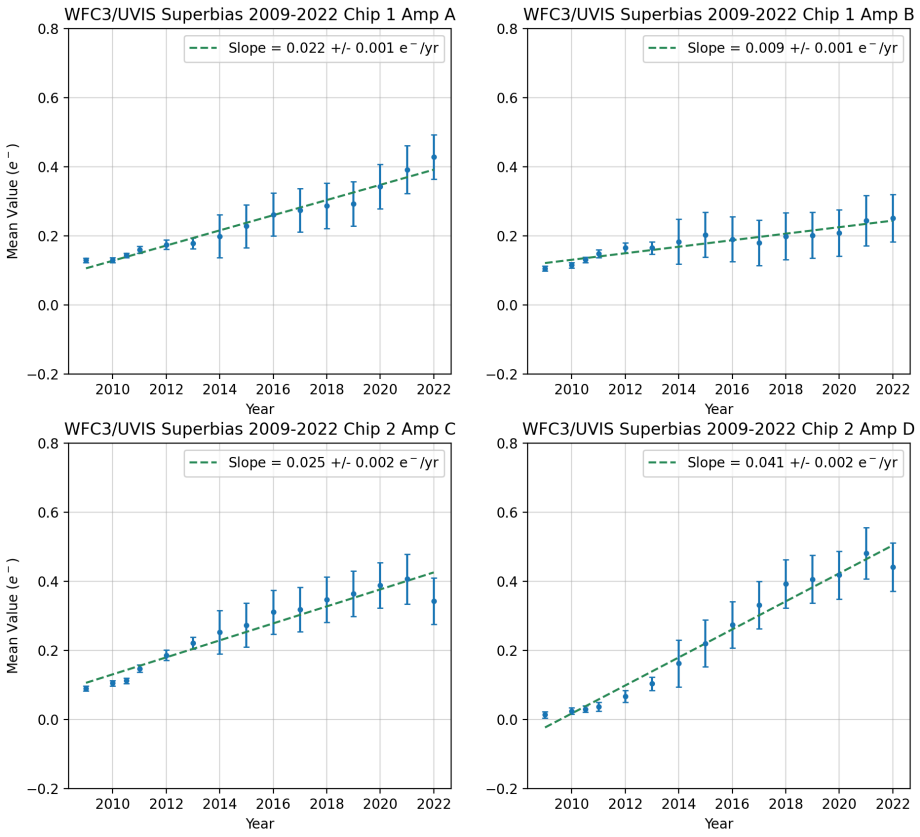

Figure 11. The average superbias value of the 2009-2022 superbias for amps A-D. The error bars are the standard error of the mean based on the number of bias exposures used to create the superbias (shown in Table 3). The dashed green lines are the best fit of a first order polynomial to the data. The slopes per amp represent the average rate of increase per year. The average rate of increase in the superbias level per chip is $0.016 \pm 0.001\ e^-/yr$ and $0.033 \pm 0.002\ e^-/yr$ for UVIS 1 and 2 respectively.

	Year	UVIS 1 Mean ($e-$)	UVIS 1 Std. ($e-$)	UVIS 2 Mean ($e-$)	UVIS 2 Std. ($e-$)	Number of Exposures
0	2009	0.12	0.01	0.05	0.01	494
1	2010a	0.12	0.01	0.06	0.01	492
2	2010b	0.14	0.01	0.07	0.01	524
3	2011	0.15	0.01	0.09	0.01	347
4	2012	0.17	0.01	0.13	0.02	246
5	2013	0.17	0.02	0.16	0.02	219
6	2014	0.19	0.06	0.21	0.07	52
7	2015	0.22	0.06	0.25	0.07	52
8	2016	0.23	0.06	0.29	0.07	53
9	2017	0.23	0.06	0.33	0.07	52
10	2018	0.24	0.07	0.37	0.07	51
11	2019	0.25	0.07	0.39	0.07	52
12	2020	0.28	0.07	0.40	0.07	52
13	2021	0.32	0.07	0.44	0.07	48
14	2022	0.34	0.07	0.39	0.07	52

Table 3. 2009-2022 UVIS superbias statistics per chip. **Note:** The 2010 data is split into two superbias files because of the large number of exposures. The uncertainties are represented by the standard error of the mean, $\frac{\sigma}{\sqrt{Number\ of\ exposures}}$ where σ is one standard deviation of the pixel values.

The gradual rise in the superbias level is associated with increasing dark current and CTE losses in the WFC3/UVIS detector. Both are byproducts of high energy radiation (e.g. CRs) damaging the lattice structure of the CCDs over time, increasing the number of hot pixels and causing electrons to be caught in "charge traps" during the readout process. The readout time when using UVIS in the full-frame, four-amp readout mode is approximately 96 seconds. Each chip starts by reading out the row closest to the amplifiers and finishes with the row farthest from the amplifiers (see Figure 1), with the last row taking a full 96 seconds to reach the serial register. Readout dark current accumulates in the detector during this time, and increases with distance from the amplifiers, so the rows farthest from the amplifiers accumulate the most readout dark. Electrons in pixels farther from the readout amplifier will also encounter more traps since they have to travel a greater distance. The trapped charge is released later in the readout process resulting in trails of charge that extend out from sources in the anti-readout direction. In addition to experiencing greater readout dark current and amount of charge traps, the pixels farthest from the amplifiers will also encounter more CRs as they wait to be read out. Although most CRs are masked when we combine the FLTs together, smeared out trails can go undetected and may remain in the final superbias image. CTE trails from hot pixels and CRs artificially increase the measured level in the superbias.

To understand the impact of CTE trails and readout dark on the superbias level we performed a similar analysis as Kuhn and Khandrika (2019), by comparing the average pixel value in the first 200 rows per amp with the last 200 rows per amp for every superbias from 2009-2022 (Figure 12). The average rate of increase in the first 200 rows read by the amplifiers for amp A is $0.003 \pm 0.002\, e^-/yr$, for amp B is $-0.002 \pm 0.000\, e^-/yr$, for amp C is $0.013 \pm 0.002\, e^-/yr$, and for amp D is $0.021 \pm 0.004\, e^-/yr$. The average rate of increase in the 200

rows farthest from the amps is $0.033 \pm 0.002\ e^-/yr$ for amp A, $0.028 \pm 0.003\ e^-/yr$ for amp B, $0.046 \pm 0.002\ e^-/yr$ for amp C, and $0.050 \pm 0.002\ e^-/yr$ for amp D (summarized in Table 4). This result demonstrates how pixels farther from the amps have systematically higher values than those closer to the amps in both chips.

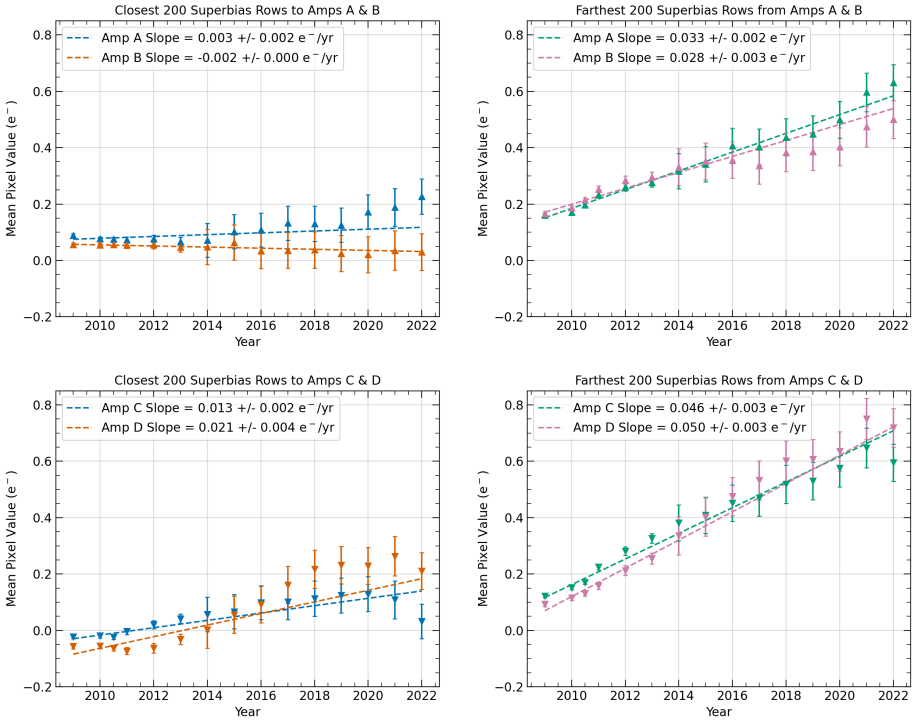

Figure 12. Left column: The mean pixel value of the 200 rows closest to the amps for amps A, B (top) and C, D (bottom). Right column: The mean pixel value of the 200 farthest rows for each amp. The measured slopes are weighted fits of the data. The rows farthest from the amplifiers accumulate the most readout dark and experience more charge traps, which causes them to have higher average values than the pixels read out first. This indicates that the pixels farthest away from the amplifiers contribute to most of the increase in the superbias level (Figure 11). If the dark current level and CTE losses were constant with time, the superbias level would be unchanging with a flat slope.

UVIS 1	***Amp A*** *(e-/yr)*	***Amp B*** *(e-/yr)*
Closest 200 Rows	*0.003 +/- 0.002*	*−0.002 +/- 0.000*
Farthest 200 Rows	*0.033 +/- 0.002*	*0.028 +/- 0.003*

UVIS 2	***Amp C*** *(e-/yr)*	***Amp D*** *(e-/yr)*
Closest 200 Rows	*0.013 +/- 0.002*	*0.021 +/- 0.004*
Farthest 200 Rows	*0.046 +/- 0.002*	*0.050 +/- 0.002*

Table 4. The average rates of increase of the 200 rows closest and farthest from the amplifiers in UVIS 1 and 2 (the slopes in Figure 12). Pixels farther from the amps have higher values than those closer to the amps in both chips.

UVIS dark frames (long 900 s exposures) are taken daily and combined into superdark reference files to monitor the dark current and number of hot pixels in the detector over time. We used the median dark current measured from the superdarks to roughly derive the expected average readout dark current per year for each amp (Figure 13). We have assumed here that the dark current rate measured from long dark exposures is the same as the readout dark current rate. It's possible this may not be the case. The measured rates of increase are $0.020 \pm 0.001\ e^-/yr$ for amp A, $0.020 \pm 0.001\ e^-/yr$ for amp B, $0.022 \pm 0.001\ e^-/yr$ for amp C, and $0.020 \pm 0.001\ e^-/yr$ for amp D. To calculate the observed residual signal due to readout dark and CTE trails in the superbias, we took the difference between the average value of the 200 rows closest to the amplifiers from the 200 rows farthest from the amplifiers. Figure 13 shows that the average of the residual signal since 2009 has increased by less than 0.5 electrons for all amps. The average rate of increase is $0.030 \pm 0.002\ e^-/yr$ for amp A, $0.028 \pm 0.002\ e^-/yr$ for amp B, $0.032 \pm 0.002\ e^-/yr$ for amp C, and $0.050 \pm 0.002\ e^-/yr$ for amp D. The expected average readout dark current is consistently less than the observed residual pixel level in the superbias, but they have similar slopes. This shows that the readout dark current is directly correlated to the increasing superbias level, but does not account for all the excess signal. As mentioned previously, a higher signal due to CTE losses also contributes to this increase.

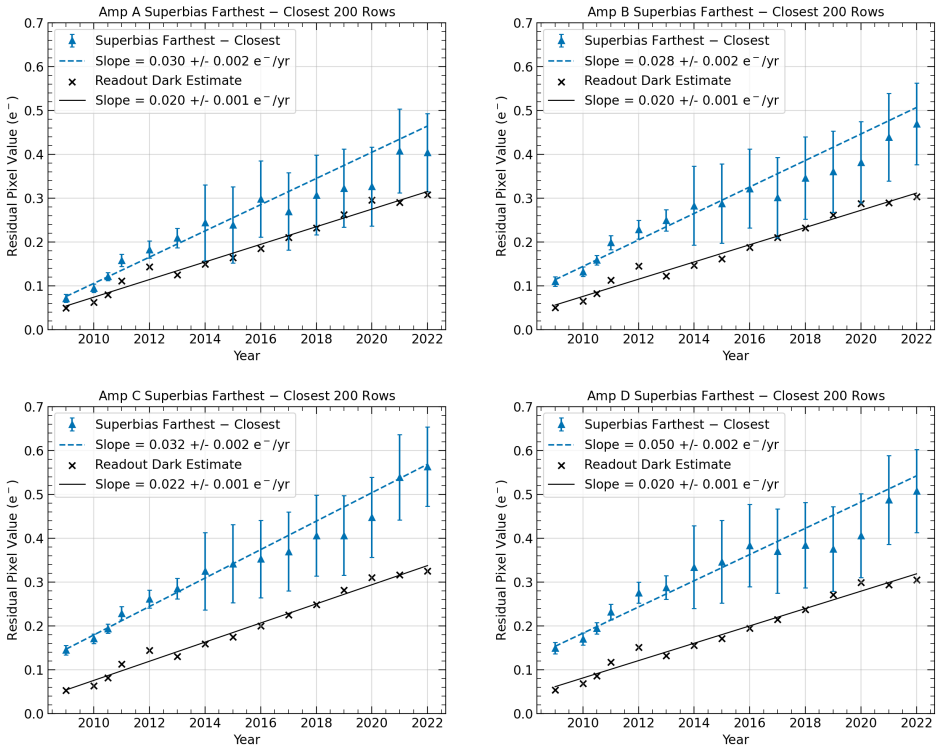

Figure 13. The blue triangles are the average residual pixel values due to readout dark and CTE trails. The black x's are the expected readout dark. The observed residual values were found by subtracting the average pixel value of the 200 rows farthest and closest to the amplifiers. The expected median readout dark was calculated by multiplying the median dark current per amp by the detector readout time, 96 s. The observed values are consistently higher than the expected readout dark, indicating that readout dark is only one contribution in the extra signal. The majority of the remaining signal is attributed to CTE loss effects.

7. Validation and Implementation

We generated the 2021 and 2022 superbias reference files using the modified WFC3 UVIS bias scripts and delivered them to CRDS and MAST. All UVIS exposures in MAST taken since January 01, 2022 have been reprocessed through `calwf3` using the 2022 superbias. We performed validation tests of the 2021 and 2022 superbiases by using them in the creation of the superdark reference files, and compared the new median dark current with the dark current using the 2020 (CRDS) superbias. Figure 14 shows the median dark current for the superdarks generated between the June-July 2022 anneal using the 2020 superbias and the 2022 superbias. There is a minimal change to the values, well within $0.5\ e^{-}/hr$ ($\leq 3\%$). This is consistent across all the tests we performed. The UVIS bias scripts will be updated and available in the spacetelescope/detectors repository on Github[1].

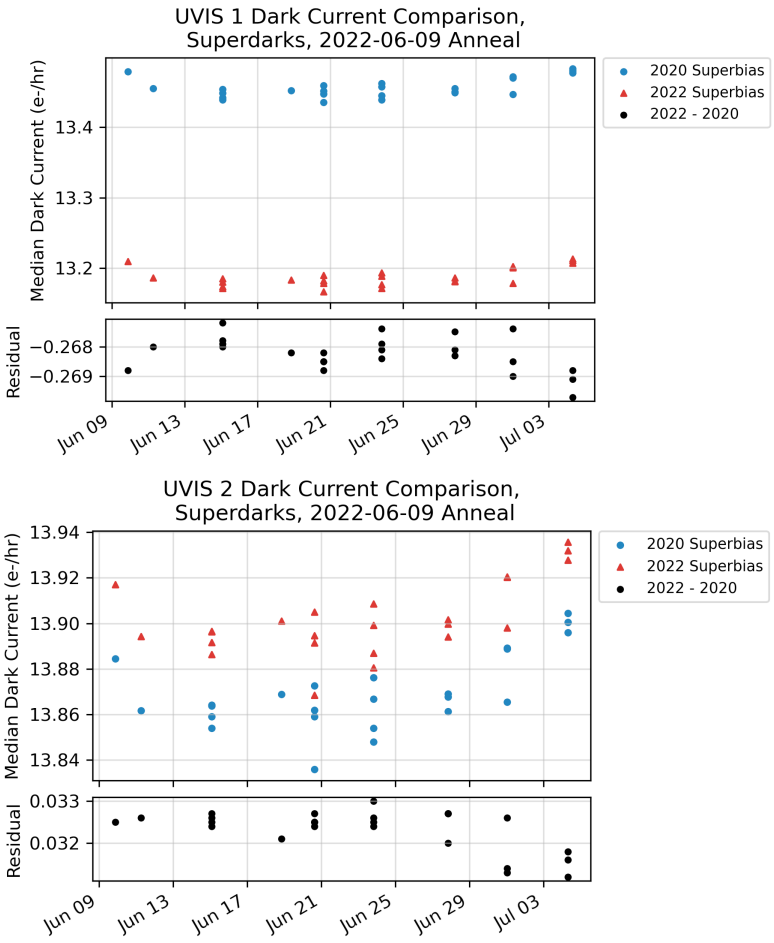

Figure 14. Median dark current of the superdarks between the June-July 2022 anneal using the 2020 and 2022 superbias for UVIS 1 (top) and UVIS 2 (bottom). The black dots represent the median dark current using the 2020 superbias subtracted from the median dark current using the 2022 superbias, which show a minimal change ($\leq 3\%$) to the values.

[1] https://github.com/spacetelescope/detectors/scripts/uvis_bias

8. Conclusion

We modified three methods in the superbias procedure (discussed in Section 3):

- Processing bias files individually rather than in an association
- CR flagging using sigma-clipping and thresholding instead of the `wf3rej` subroutine
- Replacing the NaN pixels with interpolated values instead of zero

The average 2020 superbias level increased by a negligible amount ($0.02 \pm 0.10\ e^-, \sim 5\%$) with these changes and thus will not be redelivered to CRDS. The pixel value threshold for flagging sigma-clipped pixels as CRs will be monitored as the superbias level increases. A secondary peak in the distribution of pixel values emerged for UVIS 1 of the 2021 and 2022 superbiases that have values between $\sim 2.5 - 5\ e^-$, which are mainly caused by bad partial columns. These partial bad columns will be assessed further and if necessary, added to the bad pixel tables. The average 2022 bias level is $0.37 \pm 0.07\ \mathrm{e}^-$, which is a $\sim 9\%$ increase from the 2020 superbias. The current rate of increase per year of the average superbias value is $0.016 \pm 0.001\ e^-/year$ for UVIS 1 and $0.033 \pm 0.002\ e^-/year$ for UVIS 2 which closely agrees with the previous rates of increase determined by Kuhn and Khandrika (2019).

Acknowledgements

We thank S. Baggett for providing valuable input and discussion regarding this work. We are also thankful to M. Marinelli for extensively reviewing this report and J. Anderson for providing helpful feedback regarding this analysis. Additionally, we are grateful to A. Pidgeon for performing testing and validation of the new superbiases on the UVIS superdark reference files. Finally, we thank J. Green for providing a thorough editorial review of this report.

References

Kuhn, B. and Khandrika, H. (2019). WFC3/UVIS: 2018 Superbias Reference File. *Instrument Science Report WFC3 2019-11*.

Sahu, K.C., et al., 2021, "WFC3 Data Handbook", Version 5.0, (Baltimore: STScI).

Appendix

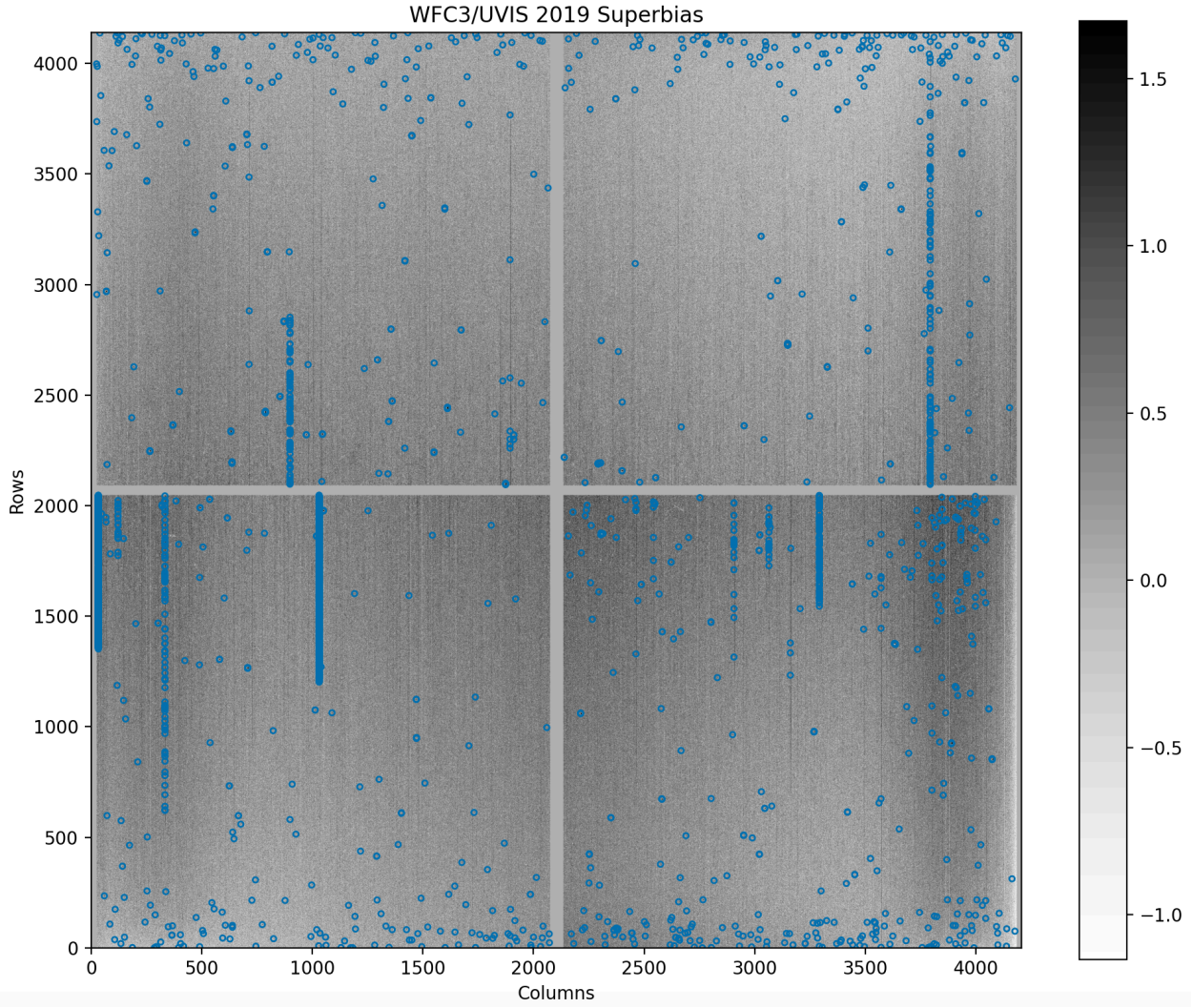

Figure 15. Image of the 2019 full-frame superbias highlighting locations of pixels ≥ 2.5 e^- with blue apertures. Most of these high value pixels are located in bad partial columns. An increase in the number of high value pixels causes a secondary peak to appear in the distribution of pixels values between 2.5-5 e^- (see Figure 7).

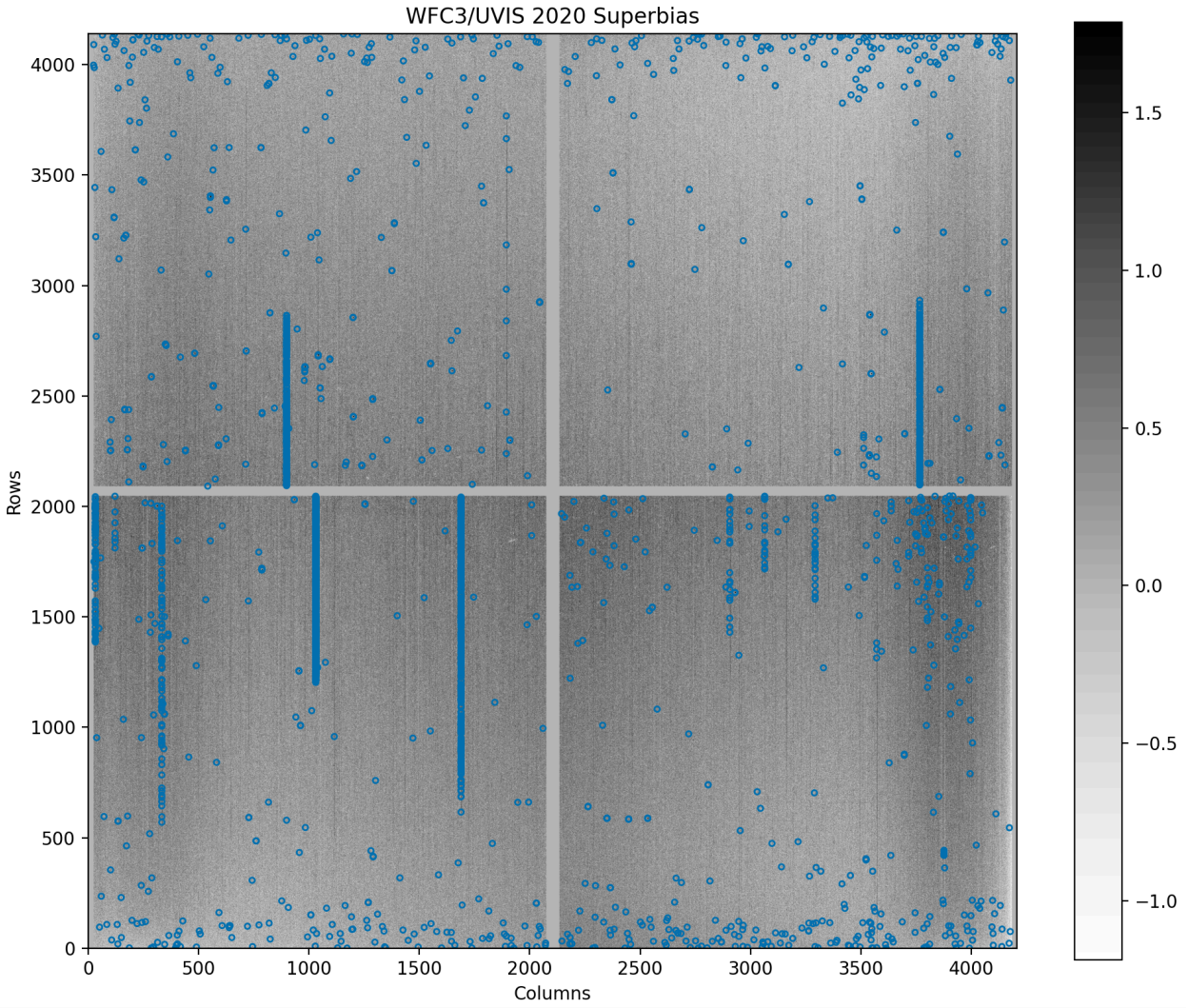

Figure 16. Image of the 2020 full-frame superbias highlighting locations of pixels ≥ 2.5 e^- with blue apertures. Most of these high value pixels are located in bad partial columns. An increase in the number of high value pixels causes a secondary peak to appear in the distribution of pixels values between 2.5-5 e^- (see Figure 7).

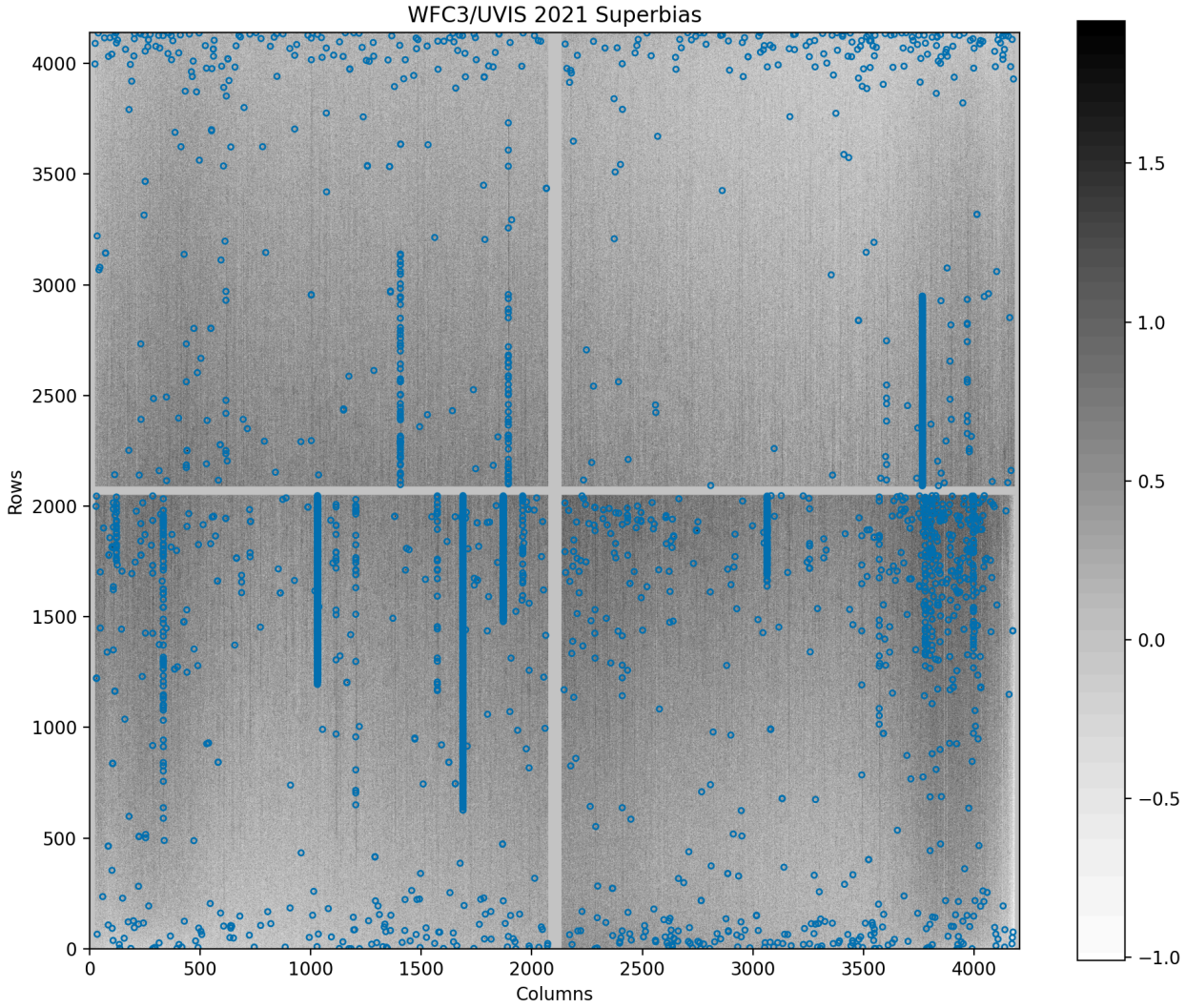

Figure 17. Image of the 2021 full-frame superbias highlighting locations of pixels ≥ 2.5 e^- with blue apertures. Most of these high value pixels are located in bad partial columns. An increase in the number of high value pixels causes a secondary peak to appear in the distribution of pixels values between 2.5-5 e^- (see Figure 7).

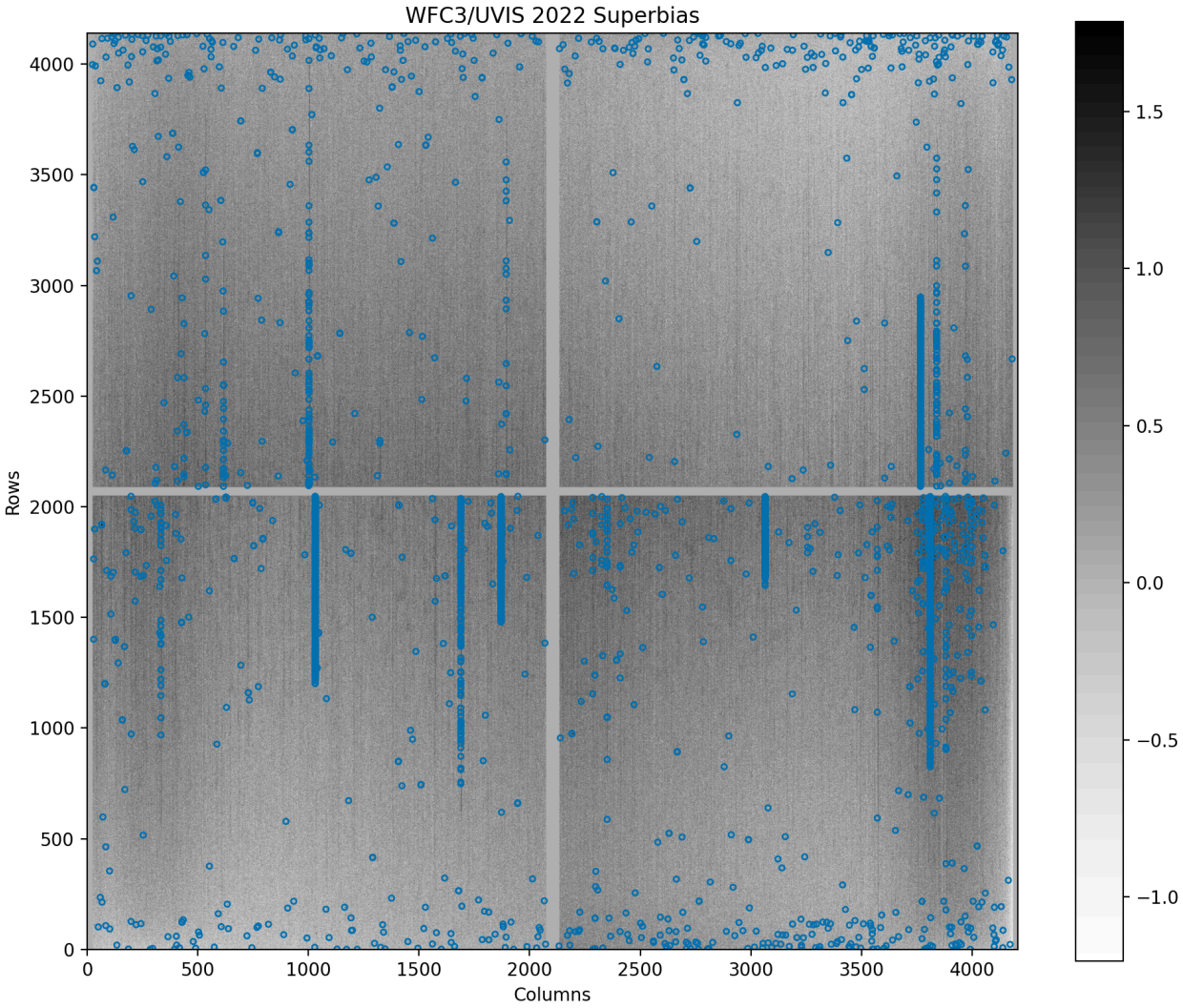

Figure 18. Image of the 2022 full-frame superbias highlighting locations of pixels ≥ 2.5 e^- with blue apertures. Most of these high value pixels are located in bad partial columns. An increase in the number of high value pixels causes a secondary peak to appear in the distribution of pixels values between 2.5-5 e^- (see Figure 7).